

On the lifetime of hot coronal plasmas arising from nanoflares

M.J. West, S.J. Bradshaw and P.J. Cargill¹

Space and Atmospheric Physics Group

The Blackett Laboratory

Imperial College

London SW7 2BW, United Kingdom

Abstract

The cooling of plasmas in closed coronal loops by thermal conduction is important when considering their detectability at X-ray and EUV wavelengths. A non-local formalism of thermal conduction originating in laboratory plasmas is used and it is shown that while the effect is unlikely to be important for loops that are in a steady state, it does play a significant role in loops that are impulsively heated (e.g. by nanoflares). Such loops are “under-dense”, and so hot electrons have a relatively long mean free path. Analytic and numerical models are presented, and it is shown that conduction cooling times are lengthened quite considerably. A comparison of various cooling times with ionisation times is also presented, and it is noted that this conductive physics may enhance the chances of observing hot nanoflare-heated plasma.

1. Corresponding author. E-mail p.cargill@imperial.ac.uk. Postal address: School of Mathematics and Statistics, University of St Andrews, St Andrews, Fife, KY16 9SS, UK.

1. Introduction

There is currently widespread interest in whether the solar corona can be heated by a large number of discrete energy releases, presumably associated with the magnetic reconnection process. Commonly referred to as the “nanoflare model” in light of the original suggestion of energy release in units of 10^{24} ergs (Parker, 1988: see also Cargill, 1994), it has been suggested that the key information about impulsive energy release (location, intensity, temporal evolution) is best seen at high temperatures, at least a few 10^6 K (e.g. Winebarger and Warren, 2004; Patsourakos and Klimchuk, 2006; Parenti *et al.*, 2006). While measurements of the corona from the SOHO and TRACE spacecraft focus on temperatures of typically 2×10^6 K or lower, new opportunities to measure high temperature coronal plasmas have arisen with the XRT instrument on *Hinode* and, later in 2008, with the AIA on SDO. However, at this time it is unclear what one could expect to actually detect (but see Parenti *et al.*, 2006). One difficulty lies in the evolution of the coronal temperature and density following an impulsive heating event. Cargill (1994) and Cargill and Klimchuk (2004) showed that a nanoflare heated corona initially is under-dense with respect to a static corona at the same temperature, and at later times is over-dense. Since the high temperature plasma is under-dense, and the intensity of an emission line scales as n^2 , one can see that there are potential detectability problems that can be compounded by instrumental sensitivity and difficulties in attaining ionisation equilibrium.

The density and temperature of an impulsively heated loop depend on the relative importance of two cooling processes: thermal conduction to the chromosphere and optically thin radiation to interplanetary space. The conductive phase drives an upflow (Antiochos and Sturrock, 1978), while the radiative phase is associated with a downflow (e.g. Cargill, Mariska, and Antiochos, 1995: hereafter CMA95; Bradshaw and Cargill, 2005). The cooling is governed by an energy equation of the form:

$$\frac{\partial p}{\partial t} = -\mathcal{P} \frac{\partial v}{\partial s} - (\gamma - 1) \left[\frac{\partial}{\partial s} \left(\kappa_0 T^{5/2} \frac{\partial T}{\partial s} \right) - n^2 R_L(T) \right] \quad (1)$$

where p , v , n and T are the pressure, velocity, number density and temperature, γ the ratio of specific heats and s the coordinate along the magnetic field. In addition there is an equation of state: $p = 2nkT$, with k being the Boltzmann constant. Here $\kappa_0 = 10^6$ ergs $\text{cm}^{-1} \text{s}^{-1} \text{K}^{-7/2}$ is the thermal conductivity coefficient, and $R_L(T)$ is the optically

thin radiative loss function. For a loss function of the form $R_L(T) = \chi T^{-1/2}$ (a common approximation between 10^5 and 10^7 K: Priest, 1982), one can show that a loop of half-length L will cool by conduction and radiation with characteristic times τ_c and τ_r , and their ratio τ_c/τ_r defined as (CMA95):

$$\tau_c = \frac{3nkL^2}{\kappa_0 T^{5/2}}, \tau_r = \frac{3kT^{3/2}}{\chi n}, \frac{\tau_c}{\tau_r} = \frac{\chi n^2 L^2}{\kappa_0 T^4}. \quad (2)$$

This shows that conductive cooling dominates for hot, tenuous (under-dense) loops, and radiative cooling dominates for cool, dense loops. If we consider ‘‘typical’’ parameters following impulsive heating ($T = 10^7$ K, $n = 10^9$ cm⁻³, $L = 2 \times 10^9$ cm), we find $\tau_c = 10$ sec. Thus any hot source may be short lived. A further consequence is that this cooling time may be less than the time needed to create the ionisation states that is required to infer the presence of hot plasmas.

This paper provides an assessment of the possible lifetime of hot, impulsively-heated coronal plasmas in active region (non-flaring) loops. In particular, we focus on the usual description of conductive losses which relies on the Spitzer-Harm (hereafter SH: Spitzer and Harm, 1953) formalism that assumes a short electron mean free path. This assumption has been sporadically questioned over the years, especially in the context of the cooling of impulsively-heated flare plasmas (e.g. Karpen and DeVore, 1987, Ljepojevic and MacNiece, 1989), but not in the context of impulsive nanoflare heating. Since violation of the SH assumption increase cooling times, it is important to assess its effect.

Section 2 introduces two alternative models of conductive cooling: the so-called ‘‘free-streaming’’ model, and the non-local model. In Sections 3 and 4 we assess these for a range of loop conditions immediately following impulsive heating. In Section 5, we discuss the cooling times with respect to the times needed to create the highly ionised states needed to infer high coronal temperatures.

2. Conductive cooling models

The classic theory of conductive cooling was developed by Cohen, Spitzer and Roulty (1950) and Spitzer and Harm (1953), and involves a solution of the Boltzmann

equation for a distribution function that deviates weakly from Maxwellian due to a temperature gradient with a characteristic scale of L_T . We define the electron mean free path in an electron-proton plasma as:

$$\lambda = (kT_e)^2 / 8\pi n_e e^4 \ln \Lambda = (V_e / \omega_e)^4 (2\pi m / \ln \Lambda) \text{ cm},$$

where $\ln \Lambda$ is the Coulomb logarithm, taken as having a value of 20, and V_e and ω_e are the electron thermal speed and electron plasma frequency respectively and T_e the electron temperature. The SH model is valid for $\lambda/L_T \ll 1$ (e.g. Luciani, Mora, and Virmont, 1983; Karpen and DeVore, 1987; Ljepojevic and MacNiece, 1989), where the inequality suggests that terms of order $(\lambda/L_T)^2$ can be neglected. However, for electrons in the tail of the distribution, SH will eventually fail for most values of λ/L_T since these energetic electrons travel large distances ($\gg \lambda$) before interacting with the background plasma.

A number of approaches have been made to address deviations from SH conduction. If we define the SH heat flux as $q_{SH} = \kappa_0 T^{5/2} dT/ds$, the simplest approach involves recognising that there is a maximum heat flux at each location when the electrons are said to “free stream”: $q_{fs} = 0.5nkTV_e$. In fact for temperatures in the range of a few MK, as considered in this paper, this condition is only met in very tenuous coronal plasmas, of order 10^8 cm^{-3} (see Bradshaw and Cargill, 2006 for a further discussion and full numerical simulations of this regime, and Patsourakos and Klimchuk, 2005 for further simulations of nanoflares when free-streaming is included).

However, other effects can lead to a deviation from SH conduction. Luciani, Mora and Virmont (1983) used results from laser plasmas to suggest that a conduction front arising from impulsive heating was modified by the streaming of very high energy electrons ahead of the front. In the context of the corona, this means that high energy electrons would move ahead of the conduction front into cooler ambient plasma. This “non-localisation” of the conduction led to the formalism described below in which the heat flux at any one point is determined by the temperature and density structure of the entire atmosphere under consideration. This approach was implemented into numerical models of solar flare plasmas (Smith, 1986; Karpen and DeVore, 1987) who showed significant delays in the cooling of flare plasma, and consequent plasma

upflows. Ljepojevic and MacNiece (1989) compared a solution of the Fokker Planck equation with a number of analytical heat flux limiting scenarios, including that of Luciani, Mora and Virmont. They showed that for models of a flare the approach of Luciani, Mora and Virmont was the most satisfactory.

Luciani, Mora and Virmont (1983: see also Luciani, Mora, and Pellat, 1985) express the non-local flux as:

$$q_{NL}(s) = \int q_{SH}(y)w(s, y)dy \quad (3)$$

where

$$w(s, y) = \frac{1}{2\lambda_{NL}(y)} \exp\left[-\frac{1}{\lambda_{NL}(y)n(y)} \int_y^s n(z)dz\right], \quad (4)$$

y and z are dummy variables, and the integration in Equation (3) is over the entire loop length. The quantity $\lambda_{NL}(y) = \phi\sqrt{2}\lambda(y)$ is an “effective” electron mean free path (Luciani, Mora, and Virmont, 1983) for an electron-proton plasma. The coefficient $\phi = 32$ was derived from the Fokker-Planck simulations of Luciani, Mora, and Virmont, and Ljepojevic and MacNiece argue that ϕ should be smaller in regions of lower temperature. This is because λ of the near-thermal electrons is otherwise over-estimated. Luciani, Mora, and Virmont also noted that Equation (3) reduced to the correct SH flux in the limit of very short mean free path at all locations.

3. Application to coronal energy balance models

In this section we explore in simple terms the implications of non-local heat conduction for coronal energy balance models. Throughout this paper we make the assumption that the heating takes place near the top of a loop (or strand). Using the equation of state we can write $\lambda = (kT_e)^3 / 4\pi p e^4 \ln \Lambda$, so that the plasma at the top of a loop has the largest values of λ . For SH conduction to be valid we would expect that the ratio $\alpha = \lambda/L$ be small, where L is the loop half-length (we assume L and L_T are the same). We find

$$\alpha = (kT_e)^3 / 4\pi p L e^4 \ln \Lambda, \quad (5)$$

and can insert some simple models that relate the coronal temperature to the pressure and length into Equation (5). For example, the Rosner, Tucker, and Vaiana (1978) scaling law, which applies to loops with steady, spatially uniform heating, states that $(kT)^3 = pL(\chi k^4 / 4\kappa_0)^{1/2}$, and on setting $\chi = 6 \times 10^{-20}$, we find $\alpha = 2 \times 10^{-4}$, which suggests that SH conduction is likely to be valid (see also Ciaravella, Peres, and Serio, 1991). It is only for high loops that additional stratification decreases the validity of SH conduction in steady state (Ciaravella, Peres, and Serio, 1991, 1993).

On the other hand, impulsive heating models do not initially have a simple relationship between temperature and density. A heating event can, in principle, occur in a loop structure with arbitrary temperature and density and, as noted in the Introduction, impulsively-heated loops are initially underdense with respect to a steady-state model. This will lead to larger values of λ . However, the cooling of such loops, as well as the conduction-driven upflows, will lead to SH eventually becoming the correct description. The nanoflare heating model of Cargill (1994) predicts that at the start of the main conductive cooling phase, $T^3 = 10^{10} Q(1 + \xi) / A_h$ and $3knT = Q(1 + \xi) / 2AL$, where Q is the nanoflare energy, A_h is the cross-sectional area of the loop or strand being heated and ξ is the ratio of the pre-nanoflare thermal energy in the loop to the nanoflare energy. In the expression for T , the numerical factor arises from the details of the model of Antiochos and Sturrock (1978). Here we find that $\alpha = 6 \times 10^{-3}$, independent of all loop parameters. Studies of non-local conduction suggest that it becomes important for such values of α .

4. Solutions for non-local conduction for simple heating scenarios

To address the limitations of SH conduction, we consider loop cooling using two models. The first, discussed in Section 4.1, assumes that the cooling is static. This implies that the heat flux into the chromosphere is all radiated away (Antiochos and Sturrock, 1976). The second model allows the lower atmosphere to respond to the heat flux by driving an upflow (“chromospheric evaporation”: Antiochos and Sturrock, 1978), and is discussed in Section 4.2.

4.1 Static Cooling

In the absence of flows, the loop pressure is spatially constant, and the initial density profile $n(s)$ does not evolve in time. The static heat conduction equation is solved:

$$3nk \frac{\partial T}{\partial t} = \frac{\partial q_{NL}}{\partial s}, \quad (6)$$

with the non-local flux calculated from Equation (3): as noted earlier, the SH case arises in the limit of short mean free path. While this approach ignores the effect of radiation in the lower atmosphere, it has the merit of isolating the conduction physics. The initial loop temperature and heat flux profiles are described by the static conductive cooling model of Antiochos and Sturrock (1976):

$$T = T_0 \left(1 - (1 - T_b/T_0) s^2 / L^2\right)^{2/7}, \quad q_{SH} = \frac{4\kappa_0 T_0^{7/2} s}{7L^2} (1 - T_b/T_0),$$

$$L_T^{-1} = \frac{4s}{7L^2} (1 - T_b/T_0) \left(\frac{T_0}{T}\right)^{7/2}$$

with T_b and T_0 the base and apex temperatures and where the loop extends from $-L$ to L , with $s = 0$ at the apex. We consider cases where $T_b = 10^4$ K and $2L = 2 \times 10^9$ cm.

Equations (3) and (6) were solved numerically to give the temperature and non-local heat flux throughout the loop as a function of time. Although symmetry was not explicitly required about the apex, it was maintained in all cases. Two sample results are shown in Figure 1 with initial apex temperatures and densities of 6×10^6 K, 5×10^9 cm⁻³ (panels a and b) and 10^7 K, 10^9 cm⁻³ (panels c and d). These densities are respectively a factor of 20 and 400 lower than that expected in a steady-state uniformly heated loop at the same temperature. The mean free paths at the loop apex are 50 and 700 km, whereas $L_T = 1.75L = 1.75 \times 10^4$ km giving values of the parameter α of 0.003 and 0.04. Figures 1a and 1c show the temperature and Figures 1b and 1d the heat flux. Results for SH (non-local) conduction are shown using dashed (solid) lines. In the heat flux plots, the left (right) axis corresponds to the SH (non-local) conduction, required because of the large differences in their values when non-local conduction is important. Finally, the sequence of lines in each plot denotes different times. Both cases are run until the apex temperature in the non-local model has fallen by a factor of e (defined as the non-local cooling time: τ_{NL}). The five lines on each plot are shown at $0.2\tau_{NL}$, $0.4\tau_{NL}$, \dots , τ_{NL} , so that one is comparing the profiles at the same times. For Fig 1a,b $\tau_{NL} = 579$ s., and for Figure 1c,d, $\tau_{NL} = 254$ s.

The corresponding SH cooling times (i.e. time for the apex temperature to decline by e in the SH model) are 487 s and 27 s. respectively.

The first case shows little difference in the cooling times but we see that there are differences in the heat flux structure near the loop ends. This is due to the non-local conductivity formalism modelling very energetic electrons streaming from the loop apex to the footpoints, and is a manifestation of the non-local transport. The second case shows clearly the effect of the non-local cooling. One can see the very fast initial SH cooling, or alternatively the slow non-local cooling (note the curves for $0.2\tau_{\text{NL}}$). Note also the different temperature profiles. Non-local conduction leading to flattening (i.e. more isothermal), at least at higher temperatures, as well as some heating near the base due to the energetic electrons that run ahead of the main conduction front. One can also see that the non-local inhibition is important for a while, but as the temperature falls, SH cooling takes over, leading to a more rapid temperature decay (contrast the results at $0.8\tau_{\text{NL}}$ and $t = \tau_{\text{NL}}$).

Figure 2 summarises the results for static cooling. We have solved Equations (3) and (6) for a series of 361 cooling loops with a grid of initial apex temperatures distributed between 10^6 and 10^7 K, and initial apex densities between 10^9 and 10^{10} cm^{-3} . This parameter range gives initial apex mean free paths in the range 0.7 – 700 km. The top four panels show the ratio of the SH to non-local cooling times ($\tau_{\text{SH}}/\tau_{\text{NL}}$: approximately always < 1) where a contour plot has been generated from the data points. Four loop lengths ($2L$) are considered of 10^9 , 2×10^9 , 3×10^9 and 4×10^9 cm (panels a – d respectively). We see that as T increases and n decreases, the role of non-local conduction becomes more important, as would be expected. For short loops, the SH conductive cooling time can be in error by up to a factor of five. As the loop length increases, the ratio increases, although still differs significantly from unity. For a given T and n , the mean free path is obviously independent of loop length, so that longer loops will have a smaller ratio of the parameter α (Equation (5)), and so be closer to SH.

The starred curve on the left of each panel denotes the combinations of T and n expected from a steady-state loop (see Section 3). It is clear that this regime does

indeed correspond to SH conduction being an adequate description. Note also that for parameters to the left of this curve, radiative cooling will be at least as important as conduction. This is because a steady-state loop has approximately equal radiative and conductive losses, and moving to the left (decreasing temperature) decreases (increases) the radiative (conductive) cooling times. To the right of the starred curve, cooling rapidly becomes conduction-dominated. The solitary star on the right denotes the initial state of cooling given by the nanoflare model discussed in Section 3 where $Q = 2.5 \times 10^{24}$ ergs and $A_h = 5 \times 10^{13}$ cm². This is always located in a region of T-n space where non-local effects modify the ratio considerably. [Note that in panel (a), this nanoflare state is located to the right of the right hand axis, and so does not appear. The temperatures that correspond to the onset of free-streaming heat conduction (e.g. Patsourakos and Klimchuk, 2005; Bradshaw and Cargill, 2006) are many times 10^7 K. Thus, the non-local effects discussed here are important long before free-streaming becomes a factor.

The ratio of cooling times does not tell the whole story. For example, the ratio can be small, but cooling using either approach can still be sufficiently fast that the lifetime of the hot plasma may still be too short to be measurable. Thus, the lower panels of Figure 2 show the difference in the cooling times ($\tau_{NL} - \tau_{SH}$ in seconds). The notation is similar to the upper panels. For short loops there is an interesting pattern. The large values of the difference at lower right are due to the fast SH cooling, and significant non-local inhibition at high temperature and low density (the most collisionless regime). The longer differences lying in a band extending upwards from the lower left occur for longer absolute values of both cooling times (and ratios nearer to unity). Here the non-local effect is weaker at any given time, but cumulatively leads to significantly longer cooling. As the length is increased, the large differences at lower right move away from the parameters studied to even lower densities but the band feature is preserved. It is important to note that differences of a hundred seconds or more are likely to be significant in assessing the detectability of hot sources (see later).

4.2 Evaporative Cooling

The second case addresses conductive cooling in an evaporative loop (e.g. Antiochos and Sturrock, 1978). For subsonic flows, it can be shown that the loop pressure is constant in space and time (Antiochos and Sturrock, 1978). The coronal density then increases as the loop cools which leads to (a) longer cooling times and (b) shorter mean free paths. Analysis of the energy and mass conservation equation leads to:

$$\frac{5p}{2T} \frac{\partial T}{\partial t} = \frac{\partial q_{NL}}{\partial s} - \frac{q_{NL}}{T} \frac{\partial T}{\partial s} = T \frac{\partial}{\partial s} \left(\frac{q_{NL}}{T} \right). \quad (8)$$

In the limit of SH conduction, this is a modified diffusion equation. We solve Equation (8) using q_{NL} in all cases.

The form of the first equality in Equation (8) also indicates that evaporation increases the cooling time. Figure 3 shows the ratio of the cooling times in the same format as Figure 2. The overall conclusions are similar, though for the same initial states the differences between the two cooling times are smaller than at constant density. This is to be expected since as the density increases during constant pressure cooling, the mean free path decreases, and the cooling will tend towards SH.

The two cases of constant density (constant pressure) cooling represent extremes: in the former (latter) all (none) of the conducted energy is radiated from the lower atmosphere. We have performed a simulation using the one dimensional HYDRAD hydrodynamic code (see Bradshaw and Mason, 2003 for details) of a loop with initial temperature of 8×10^6 K, density of $5 \times 10^8 \text{ cm}^{-3}$ and length 2×10^9 cm. This code treats each of conduction, radiation and mass flows. Figure 4 shows the temperature at the top of the loop for SH (solid line) and non-local (dash-dot line) conduction. It is seen that the delay in the cooling in the non-local model is of order 25 secs, demonstrating that the delayed cooling is preserved in full hydrodynamical calculations.

Although the detailed plasma flows generated are beyond the scope of this paper, this Figure shows interesting differences between the two conductivity models as demonstrated by the temperature around 80 s. Local conduction drives a gentle evaporative upflow that permits a smooth decrease in temperature. On the other hand, the non-local case has a transient temperature increase at 80 s. This arises from the

interaction of the fastest electrons with the chromosphere, driving an upflow from each footpoint, similar to what happens in flares (e.g. Karpen and DeVore, 1987). These upflows collide at the loop summit, leading to transient compressive plasma heating.

5. Can ionisation states corresponding to nanoflare temperatures be created?

Figure 5 shows the characteristic time-scale for Fe XVIII to form Fe XIX by ionisation, as a function of density and temperature. The time-scales are obtained using the ionisation rate calculations of Mazzotta *et al.*, (1998). If we look at typical nanoflare parameters (near 10^7 K and 10^9 cm⁻³), we see that the time-scale is between 10 and 100 secs. If the initial plasma is in a cooler state than that at which Fe XVIII has its peak, then the time to create the Fe XIX state will be longer, though the initial stages should be fast for temperatures of order 10^7 . For SH cooling, it is evident that the ionisation and cooling times are at best comparable, and in less favourable scenarios, the plasma will have cooled long before the relevant states have been established. The delays in the cooling of the corona of tens to hundreds of secs due to the non-local effects can thus be significant in keeping the corona hot enough for long enough to create the required ionisation states.

6. Discussion

In qualitative terms, the effect of the non-local heat flux in an impulsively-heated loop is quite easy to assess. The rate of conductive cooling is slowed, the transition to radiative cooling occurs at a higher temperature and lower density, and the radiative cooling is also slower (see CMA95). What are the consequences for what is (or is not) seen in the corona?

It is now becoming clear that hot coronal plasma components may be a key factor in identifying the heating process (e.g. Patsourakos and Klimchuk, 2006; Parenti *et al.*, 2006). The lifetime and intensity of such plasmas are determined almost entirely by conductive cooling. Prolonging the lifetime of such a component, as happens for most nanoflare scenarios (Figures 2 and 3) will increase the detectability, since more photons can be detected over a given integration period, and there is also an increased

probability that ionisation equilibrium can occur, so creating ions characteristic of the temperature.

However, these results have focussed on a single heating event in the single strand of a nanoflare-heated ensemble of strands, and also assume that a strand cools down before any reheating occurs. What changes can be expected when multiple nanoflares within a coronal volume are considered? The key parameter in assessing this is the ratio of the “repetition time” of a nanoflare (τ_{nano}) in any particular strand to the total (conductive + radiative) cooling time (τ_{cool} ; Cargill, 1993). When $\tau_{nano} > \tau_{cool}$, each strand heats and cools independently, so any signal is just the convolution over many hot sources whose evolution is as described in this paper. For the opposite inequality, a strand is reheated before it can completely cool. For a given nanoflare energy, this leads to lower initial temperatures and higher densities (Cargill, 1994), thus taking the conduction closer to classical SH.

As a closing comment, it appears that detectability of nanoflares or other hot, transient coronal plasmas could be enhanced by observations with low spatial resolution and long integration times. We note that measurement of coronal plasmas over a wide temperature range has long been a priority of stellar astronomers (e.g. Sans-Forcada, Brickhouse, and Dupree, 2003; Cargill and Klimchuk, 2006), and encourage the solar community to also focus on this regime, preferably by studying a continual range of Fe lines, as was possible with the Extreme Ultraviolet Explorer (EUVE) mission.

Acknowledgement

All authors acknowledge support from PPARC: PC through a senior research fellowship, SB through a postdoctoral fellowship and MW through a studentship. We are grateful to the referee for many helpful comments. PC also acknowledges the support of the International Space Science Institute (ISSI) through its team “The role of spectroscopic and imaging data in understanding coronal heating”, and thanks the team leader, Susanna Parenti and other members for helpful discussions.

References

- Antiochos, S.K., Sturrock, P.A.: 1976, *Solar Phys.*, **49**, 359.
- Antiochos, S.K., Sturrock, P.A.: 1978, *Astrophys. J.*, **220**, 1137.
- Bradshaw, S.J., Cargill, P.J.: 2005, *Astron. Astrophys.*, **437**, 311.
- Bradshaw, S.J., Cargill, P.J.: 2006, *Astron. Astrophys.*, **458**, 987.
- Bradshaw, S.J., Mason, H.M.: 2003, *Astron. Astrophys.*, **401**, 699.
- Cargill, P.J.: 1993, *Solar Phys.*, **147**, 263.
- Cargill, P.J.: 1994, *Astrophys. J.*, **422**, 381.
- Cargill, P.J., Mariska, J.T., Antiochos, S.K.: 1995, *Astrophys. J.*, **439**, 1034.
- Cargill P.J., Klimchuk, J.A.: 2004, *Astrophys. J.*, **605**, 911.
- Cargill P.J., Klimchuk, J.A.: 2006, *Astrophys. J.*, **643**, 438.
- Ciaravella, A., Peres, G., Serio, S.: 1991, *Solar Phys.*, **132**, 279.
- Ciaravella, A., Peres, G., Serio, S.: 1993, *Solar Phys.*, **145**, 45.
- Cohen, R.S., Spitzer, L., Roulty, McR.: 1950, *Phys. Rev.*, **80**, 230.
- Karpen, J.T., DeVore, C.R.: 1987, *Astrophys. J.*, **320**, 904.
- Ljepojevic, N.N., MacNiece, P.: 1989, *Phys. Rev A*, **40**, 981.
- Luciani, J.F., Mora, P., Virmont, J.: 1983, *Phys. Rev. Lett.*, **51**, 1664.
- Luciani, J.F., Mora, P., Pellat, R.: 1985, *Phys. Fluids*, **28**, 835.
- Mazzotta, P., Mazzitelli, G., Colafrancesco, S., Vittorio, N., 1998, *Astron & Astrophys. Supp.*, **133**, 403.
- Parenti, S., Buchlin, E., Cargill, P.J., Galtier, S., Vial, J-C.: 2006, *Astrophys. J.*, **651**, 1219.
- Parker, E.N.: 1988, *Astrophys. J.*, **330**, 474.
- Patsourakos, S., Klimchuk, J.A.: 2005, *Astrophys. J.*, **628**, 1023.
- Patsourakos, S., Klimchuk, J.A.: 2006, *Astrophys. J.*, **647**, 1452.
- Priest, E.R.: 1982, *Solar Magnetohydrodynamics*, Kluwer.
- Rosner, R., Tucker, W.H., Vaiana, G.S.: 1978, *Astrophys. J.*, **220**, 643.
- Sans-Forcada, J, Brickhouse, N.S., Dupree, A.K.: 2003, *Astrophys. J. Supp.*, **145**, 147.
- Smith, D.F.: 1986, *Astrophys. J.*, **302**, 836.
- Spitzer, L., Harm, R.: 1953, *Phys. Rev.*, **89**, 977.
- Winebarger, A.R., Warren, H.P.: 2004, *Astrophys. J.*, **610**, L129.

Figure Captions

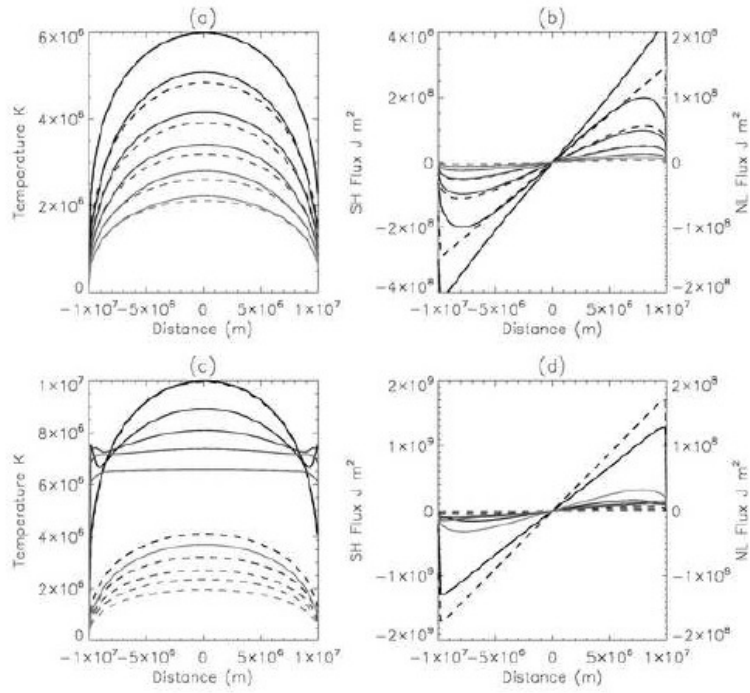
Figure 1. The temperature (1a,c) and heat flux (1b,d) profiles for the cooling of two loops at a sequence of different times. The upper: Figures 1a,b (lower: Figures 1c,d) panels have initial temperatures and densities of 6×10^6 K, $5 \times 10^9 \text{ cm}^{-3}$ (10^7 K, 10^9 cm^{-3}). In all panels, non-local (SH) cooling is represented by solid (dashed) lines. The left (right) axis of Figs 1b,d correspond to the SH (non-local) heat flux). Each plot shows 6 different times: $0, 0.2\tau_{\text{NL}}, 0.4\tau_{\text{NL}}, \dots, \tau_{\text{NL}}$, where τ_{NL} is 579 (1a,b) and 254 (1c,d) s.

Figure 2. The upper four panels (2a-d) show the ratio of the classical (τ_{SH}) to non-local (τ_{NL}) cooling times for the case of conductive cooling at constant density. A range of temperatures and densities and four loop lengths ($2L$) are shown with $2L = 10^9$ cm (2a), 2×10^9 cm (2b), 3×10^9 cm (2c) and 4×10^9 cm (2d). The lower panels (2e-h) show the difference in the cooling time (in seconds) for the same four cases. On all panels the starred line (black or white as required for clarity) on the left denotes the location in (T-n) space of steady-state equilibria, and the star on the right of figures 2f-h denotes the T-n pair corresponding to a nanoflare-heated corona.

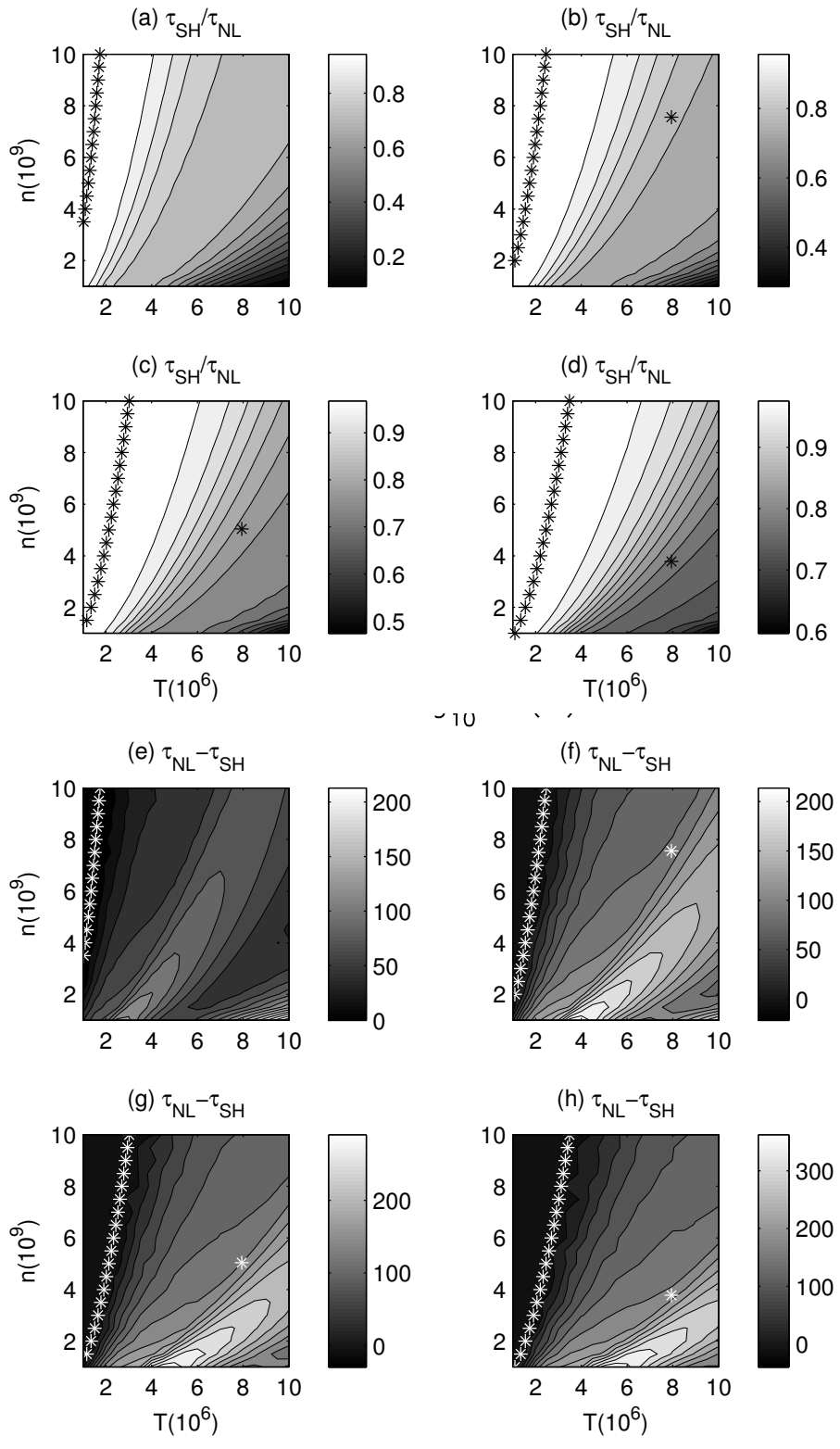
Figure 3. As Figure 2, except constant pressure conductive cooling is considered.

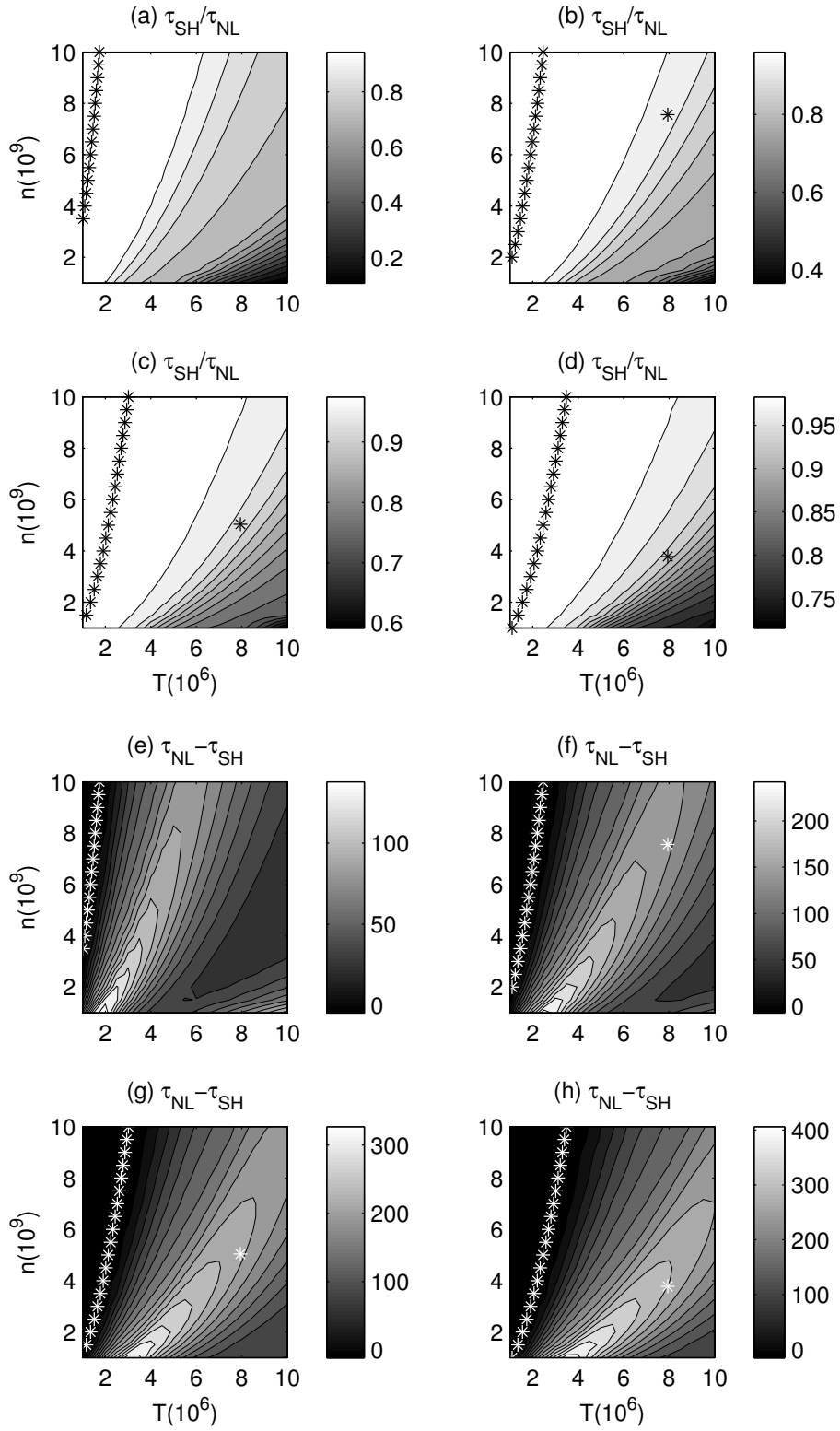
Figure 4. The apex temperature for SH cooling (solid curve) and for non-local cooling (dot-dashed line) as calculated by the HYDRAD model.

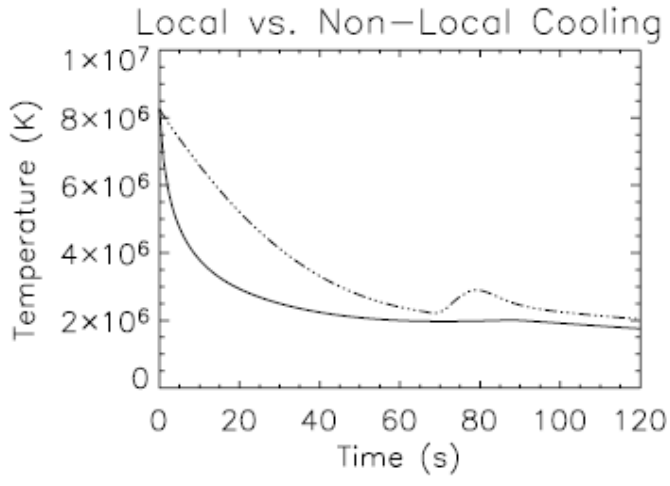
Figure 5. The ionisation timescale to go between Fe XVIII and Fe XIX as a function of temperature and density. Contours are labelled in seconds to the power ten.



X







Ionisation time-scales for Fe XVIII to Fe XIX

